Role of the van der Waals interactions and impact of the exchange-correlation functional in determining the structure of glassy $GeTe_4$

Assil Bouzid, Carlo Massobrio, Mauro Boero, and Guido Ori
Institut de Physique et de Chimie des Matériaux de Strasbourg, University of Strasbourg - CNRS UMR 7504, 23 rue du Loess, BP 43, F-67034 Strasbourg, France

Kateryna Sykina and Eric Furet
Institut des Sciences Chimiques de Rennes UMR 6226, École Nationale Supérieure de Chimie de Rennes, Avenue du Général Leclerc, CS 50837, F-35708 Rennes, France

(Received 29 May 2015; revised manuscript received 25 September 2015; published 30 October 2015)

The structural properties of amorphous $GeTe_4$ are studied within the framework of first-principles molecular dynamics combined with density functional theory. Four different theoretical schemes are considered, each one intended to correspond to a distinct structural model. These are obtained by selecting either the PBE (Perdew, Burke, and Ernzerhof) or the BLYP (Becke, Lee, Yang, and Parr) exchange-correlation functionals and, for each one of the two, by disregarding or including van der Waals dispersion forces. Based on the comparison with experimental total structure factor $S(k)$ and total pair correlation function $g(r)$, one can infer the quantitative character of such models, thereby extracting information on the underlying structures. We found that the inclusion of the vdW forces improves the predictive power of our approach for the PBE and (to a smaller extent) the BLYP exchange-correlation functionals. Overall, BLYP performs better than PBE in reproducing the available experimental quantities, providing a tetrahedral atomic-scale network profoundly different from the one predicted by PBE, in which tetrahedral and octahedral motifs do coexist. Our work demonstrates that a careful choice of the exchange-correlation functional, combined with the account of van der Waals forces, is crucial to achieve realistic structural predictions for glassy $GeTe_4$.

DOI: 10.1103/PhysRevB.92.134208 PACS number(s): 61.43.Fs, 71.15.Pd, 72.80.Ng

I. INTRODUCTION

Amorphous $GeTe_4$ (a-$GeTe_4$) is a recurrent subsystem in an important variety of ternary phase-changing alloys including Ge and Te in their composition[1–3]. Also, a-$GeTe_4$ is a peculiar binary chalcogenide prototype because of its intrinsic thermal and optical properties [4,5] and potential applications in memory cells [6,7]. Combinations of Ge and Te at various concentrations are ubiquitous in many ternary materials of high fundamental and technological interest [8–10]. Therefore, a precise understanding of Ge-Te disordered networks structures can highlight the interplay between macroscopic properties and the underlying chemical bonding.

In spite of the availability of experimental and theoretical information on the structure of Ge_xTe_{1-x} at concentrations $x \sim 0.2$, a clear-cut description of the network topology remains elusive. By relying on state of the art atomic-scale modeling, one seeks an unambiguous picture of the nature of the connectivity in terms of specific structural units. For instance, it remains unclear whether glassy $GeTe_4$ could be better described as a tetrahedral or an octahedral network or a combination of the two [11,12].

In a seminal paper, Akola and Jones investigated disordered (liquid and glassy) GeTe and $Ge_{15}Te_{85}$ within first-principles molecular dynamics (FPMD). They adopted the Perdew, Burke, and Ernzerhof (PBE) generalized gradient approximation (GGA) exchange-correlation (XC) scheme [11]. A fourfold coordination for Ge and a threefold coordination for Te were proposed, together with a detailed structural analysis featuring voids and the lack of Te segregation. Extended results on the $Ge_{15}Te_{85}$ amorphous structure obtained from the constrained reverse Monte Carlo approach showed that the Ge occurs in both tetrahedral and defective octahedral configurations [13].

More recently, the quantitative character of DFT-FPMD approaches on telluride-based materials has been questioned by Micoulaut [14]. This author showed that substantial improvements in the structure factor and pair correlation functions of liquid $Ge_{15}Te_{85}$ can be obtained by accounting for the van der Waals (vdW) dispersion forces. Along the same lines (PBEsol XC functional and vdW forces included), the structure of a-$GeTe_4$ was found to consist of 54.6% of tetrahedral configurations [12,15]. The importance of these results stems from the observation that all available XC functionals share the general drawback of the nonaccount of long-range electron correlations responsible for van der Waals (vdW) dispersive forces. Yet, vdW interactions have been shown to be far from negligible in several condensed phases [14,16–18], and in some cases they are even essential to stabilize inorganic and organic structures that otherwise would not be stable [19] or even collapse [20].

Given these premises, two considerations are in order. First, it appears that dispersion forces are crucial at least in the case of some Ge_xTe_{1-x} disordered systems. Second, the predictive power of DFT-FPMD approaches turns out to be much lower for disordered Ge_xTe_{1-x} systems than in the case of their Ge_xSe_{1-x} counterparts. This assertion is based on a large body of DFT-FPMD results on Ge_xSe_{1-x} glasses and liquids, exhibiting quantitative agreement with experimental structural properties [21–27]. For some systems of this family (and particulary for $GeSe_2$), a crucial role was found to be played by the XC functional. This was exemplified by the improved description of the short-range Ge environment

resulting from the adoption of the Becke, Lee, Yang, and Parr (BLYP) recipe [28–30]. This scheme is expected to enhance the localized behavior of the electron density at the expenses of the electronic delocalization effects that favor the metallic character. These drawbacks are built in generalized gradient approximation (GGA) approaches having the uniform electron gas as reference system (the one due to the Perdew and Wang being an example) [31].

These considerations legitimate a theoretical effort to elucidate the structural properties of a-$GeTe_4$ by resorting to *four* different choices for the selection of the exchange-correlation functional and the account of the vdW dispersion forces. More precisely, we have produced models of a-$GeTe_4$ characterized by PBE as XC functional and no account of vdW forces (PBE hereafter), PBE as XC functional in the presence of vdW forces (PBE-vdW), BLYP as XC functional and no account of vdW forces (BLYP), and BLYP as XC functional in the presence of vdW forces (BLYP-vdW). For each of these models, we have calculated quantities that can be directly compared with experiments [total structure factor $S(k)$ and total pair correlation function $g(r)$] as well as additional structural properties (partial correlation function, bond angle distributions, coordination numbers, and local order parameters). Such an endeavor allows us to draw unambiguous conclusions on the performances of each one of these schemes, thereby providing clues on their reliability.

In short, our analysis confirms that vdW dispersion forces are instrumental in improving the accuracy of the DFT-FPMD description. The choice of the XC functional is also crucial, since BLYP not only performs better than PBE when compared to available experiments but it provides a network topology drastically different from that issued from the PBE approach.

The present paper is organized as follows. In Sec. II we provide details of our computational methodology, built on the use of two different exchange-correlation functionals and the account of vdW dispersion forces. Section III is devoted to our results and it is organized in six subsections. The first two feature the comparison between theory and experiments for the total structure factor $S(k)$ and the total pair correlation function $g(r)$ as well as the analysis of the partial pair correlation functions. Then, we move to considerations relative to the coordination numbers, for each species and for the whole system. Bond angle distributions are also described. We focus on the different network topologies obtained for the two different exchange-correlation functionals in the presence of the vdW contributions. In a final subsection, we highlight correlations between structural and electronic properties by relying on the Wannier functions formalism [32,33]. A final rationale summarizing the indications collected through our calculation is contained in Sec. IV.

II. COMPUTATIONAL METHODS

Our simulations were conducted within the Car-Parrinello (CP) [34] molecular dynamics (CPMD) approach, as implemented in the CPMD code [35]. Our DFT approach makes use of either the BLYP [36,37] or the PBE [38] XC functionals. The valence-core interaction is described by a norm-conserving pseudopotential according to the prescription of Troullier and Martins [39]. Concerning the choice of the energy cutoffs for the representation of the valence electrons in the plane-wave basis set, we were guided by the results of test calculations on the Ge-Te dimer. The total energies of a Ge-Te dimer calculated at the equilibrium distances for various cutoffs in between 20 Ry and 50 Ry lie within less than 0.5%. This ensures that any value in this interval can be adopted without loss of generality and/or accuracy. Due to a distribution of the computational effort on resources having unequal performances, we selected an energy cutoff of 20 Ry for the PBE case and of 40 RY for the BLYP case.

The Brillouin zone integration was restricted to the Γ point. Long-range dispersion forces were accounted for according to the DFT-D2 formula proposed by Grimme [40]. We stress the fact that, although empirical, such a vdW correction is a thorough DFT-based formulation in which parameters are self-consistently tuned on different functionals, including the two used in this work, and benchmarked on a wealth of different systems from simple molecules to complex reactive surfaces and chalcogenides [41–43]. No experimental parameters are included in the construction of this specific vdW correction and its inclusion does not affect at any stage the Kohn-Sham equations [44,45], thus preserving the first-principles character of all electronic structure calculations.

Quite recently, the general applicability of this recipe was questioned in the case of amorphous GeTe [46], for which a failure in improving the agreement with experiments is reported. In the framework of a seminal study on the aging mechanism in ternary phase-change materials, a more complex vdW density functional was adopted [46]. With respect to the choice made in Ref. [46] and the rationale developed herein, we anticipate that in the present case (a-$GeTe_4$) the role of the Grimme formula is far from negligible and contributes significantly to improving the performances of our level of theory.

The temperature was controlled with a Nosé-Hoover [47–49] thermostat chain [50], and an integration step of 7 au, i.e., 0.16 fs, ensured a good control of the conserved quantities all along the simulations. Also, the control of the electronic degrees of freedom was implemented along the lines pioneered by Blöchl and Parrinello [51], with choices for the target kinetic energy comprised between 0.03 and 0.05 a.u.

A first periodic system made of 185 atoms (37 Ge, 148 Te) in a cubic simulation cell of side equal to 18.30 Å was randomly generated within both the PBE and the PBE-vdW schemes. Hereafter we refer to this PBE model as *model 1*. Extended trajectories were implemented to lose memory of the initial configuration and produce a reliable amorphous structure. To this purpose, two independent thermal schedules (one for PBE and one for PBE-vdW) were produced as follows: $T = 1000$ K (15.2 ps), $T = 700$ K (15.2 ps), $T = 500$ K (15.2 ps), $T = 300$ K (35.6 ps/38.6 ps).

A second 185-atom model (*model 2*) was generated by selecting as a starting configuration one of those produced at equilibrium for model 1 in the absence of vdW contributions. Then, a run at $T = 300$ K lasting 50 ps was performed by using the BLYP XC functional while a BLYP simultaneous run using the identical starting configuration and including the vdW corrections lasted 46 ps. Due to the absence of substantial atomic rearrangements in the production of model 2 at room temperature, the results can be exploited to have

a preliminary insight on the effect of the different XC and vdW options employed. However, model 2 suffers from an insufficient phase space sampling and cannot be taken as representative of unbiased BLYP-based equilibrium properties devoid of memory of the initial conditions. To go beyond these limits and allow for a comparison between the PBE and BLYP models totally based on fully independent equilibrium trajectories, we resorted to a third model, *model 3*. Focusing on model 3, the description of the thermal cycle refers to simulations carried out independently for the BLYP and the BLYP-vdW approaches. We have taken 215 atoms (43 Ge, 172 Te) in a cubic supercell of edge equal to 19.24 Å. Initial configurations were selected from previous data on amorphous $GeSe_4$ [26]. After replacing each Se atom with a Te atom, we annealed the $GeTe_4$ structure via damped dynamics to 0 K in order to eliminate the residual forces and stresses induced by the substitution. The BLYP and BLYP-vdW structures were heated to 100 K for about 4 ps, after which the temperature was raised to 300 K and the systems allowed to equilibrate for 12 ps. In a further step, two runs at 600 K and 900 K of 22 and 20 ps, respectively, were produced to bring the systems to the liquid state. The two liquids $GeTe_4$ thereby obtained were then cooled down by decreasing the temperature to 600 K for 20 ps and, finally, at room temperature (300 K) for 32 ps.

To establish correlations between the structural features of the different glassy networks and their electronic structure, we calculated the electronic density of states (averaged over 50 trajectories) and the maximally localized Wannier functions [32,33]. Following the standard procedure, the Wannier functions and the corresponding centers are obtained as unitary transformations *on the fly* of the Kohn-Sham orbitals $\psi_i(\mathbf{r})$. Specifically, among all the possible unitary transformation, we select the one that minimizes the spread (spatial extension) of the resulting Wannier orbitals $w_n(\mathbf{r})$:

$$\Omega = \sum_n (\langle w_n|\mathbf{r}^2|w_n\rangle - \langle w_n|\mathbf{r}|w_n\rangle^2). \tag{1}$$

This leads to an iterative scheme for computing the orbital transformation:

$$w_n(\mathbf{r}) = \sum_i \left[\prod_p \exp\left(-A^p_{i,n}\right)\psi_i(\mathbf{r})\right], \tag{2}$$

where $A^p_{i,n}$ is a matrix generalization of the Berry phase connector, i the wave vector, and p is the order of the iteration as specified in Ref. [33]. The Wannier states provide in this way an unbiased method for partitioning the charge density. The information on bonding becomes then contracted into four numbers, and the center of the orbital is then defined by

$$x_n = -\frac{L}{2\pi}\mathrm{Im}\, m \ln\langle w_n|\exp[-i2\pi(x/L)]|w_n\rangle, \tag{3}$$

with similar expressions along the other two Cartesian directions, and its related spread. Here L is the length of the simulation cell along the x direction. The analysis of the Wannier functions centers with respect to the nuclear positions was successful to gain insight into the correlation between network properties and electronic structure in several disordered chalcogenides [22,52,53].

III. STRUCTURAL PROPERTIES VIA FIRST-PRINCIPLES MOLECULAR DYNAMICS

A. Comparing total structure factors and pair correlation functions

We obtain a first indication of the role of the vdW interaction on the structure of a-$GeTe_4$ by accounting for the results of model 1 and model 2. For model 1, one can consider the data as being fully representative of the PBE case, since both trajectories (with and without vdW contributions) are characterized by significant diffusion in the parent liquid state. On the contrary, in the case of model 2 (BLYP scheme), the trajectories have been produced at $T = 300$ K taking a PBE configuration as the starting point (see computational methods above).

Among the two functionals used, BLYP is the best performing in terms of intensities of the maxima and minima, the positions of the main peaks not differing significantly when comparing PBE and BLYP. In addition, the inclusion of vdW corrections on both functionals has the net effect of improving the agreement with available experiments by enhancing the first minima that become clearly more pronounced in both the total structure factors $S(k)$ and the total pair correlation functions $g(r)$ (see Fig. 1). When considering the two pairs of results PBE vs BLYP and PBE-vdW vs BLYP-vdW in reciprocal space, a notable feature is the different intensity of the first peak, higher in the PBE-vdW than in the BLYP-vdW

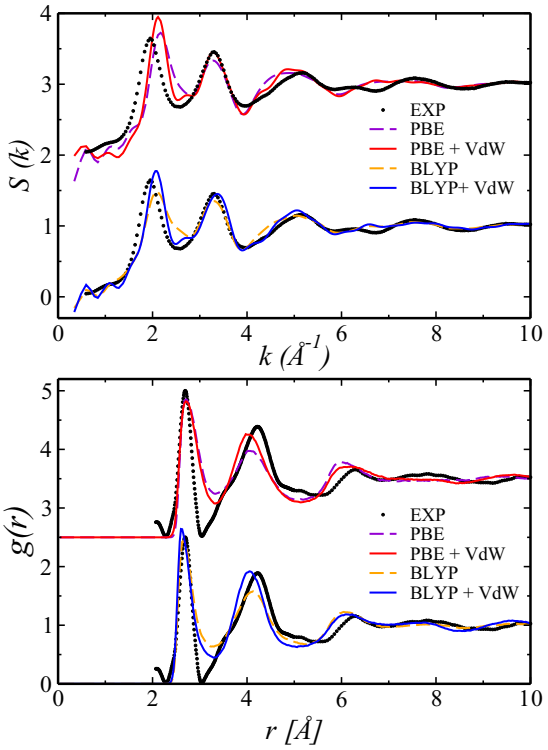

FIG. 1. (Color online) Total structure factor $S(k)$ (upper panel) and total pair correlation function $g(r)$ (lower panel) of a-$GeTe_4$ for model 1 (PBE) and model 2 (BLYP). The black dots refer to the experimental result whereas different color codes (see legend) are for the results obtained with the PBE and BLYP functionals. The comparison with experiments is based on the results of Ref. [54].

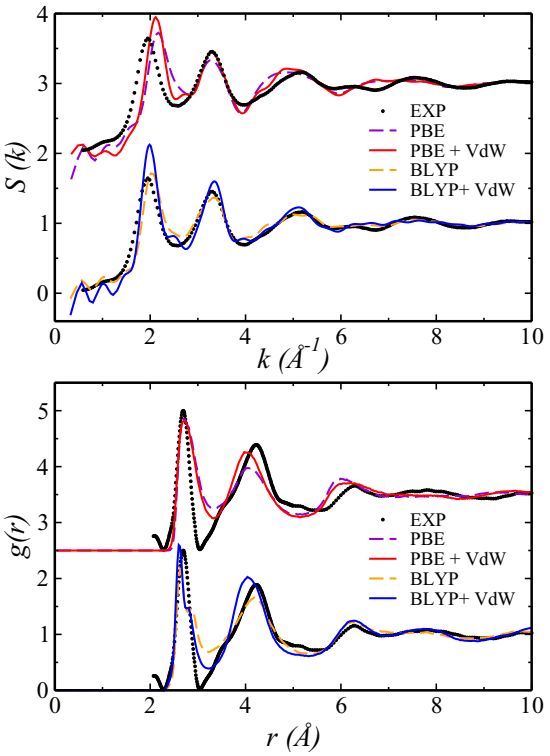

FIG. 2. (Color online) Total structure factor $S(k)$ (upper panel) and total pair correlation function $g(r)$ for a-$GeTe_4$ calculated within model 1 (PBE) and model 3 (BLYP). The black dots refer to the experimental result whereas different color codes (see legend) are for the results obtained with the PBE and BLYP functionals. The comparison with experiments is based on the results of Ref. [54].

case. In direct space, the pair correlation functions obtained by using BLYP are in better agreement with experiments [54], the overall profile approaching even better the experimental findings when the vdW contributions are accounted for. This assessment is substantiated by the use of the goodness-of-fit parameter R_χ introduced by Wright [55]:

$$R_\chi \equiv \left\{ \frac{\sum_i [g_{\rm exp}(r_i) - g_{FPMD}(r_i)]^2}{\sum_i g^2_{\rm exp}(r_i)} \right\}^{1/2}. \qquad (4)$$

R_χ takes values that are systematically lower in the BLYP case than in PBE, as such 16% (BLYP-vdW) against 22% (PBE-vdW) when considering the corresponding total pair correlation functions. Less striking (less than 1%) are the differences for a same functional with or without vdW inclusion, especially for the BLYP case.

To further substantiate these findings, we can resort to model 3, purposely constructed to obtain BLYP data at $T = 300$ K resulting from significant statistical sampling. This new set of data is the best suited to describe the effect of the XC BLYP functional on the structural properties in the absence and in the presence of the vdW forces. For the total structure factor $S(k)$ and the total pair correlation function $g(r)$, our results are given in Fig. 2.

It is worth reminding that the PBE results displayed in Fig. 2 are identical to those of Fig. 1. In direct space (pair correlation function), the BLYP-vdW combination is once again the one

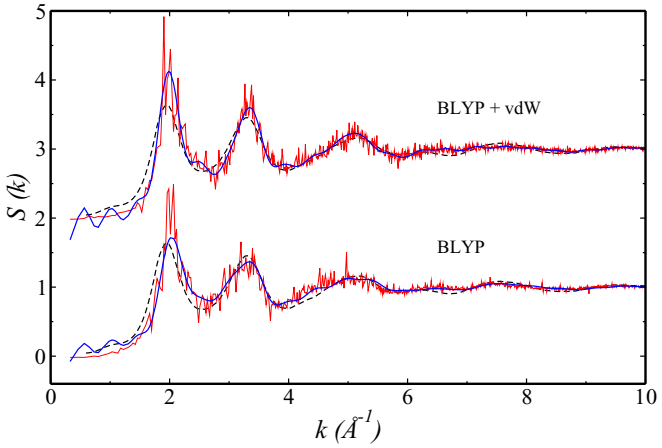

FIG. 3. (Color online) Total structure factor $S(k)$ of a-$GeTe_4$ calculated within model 3. The black dots refer to the experimental result, the solid blue curve refers to the total structure factor as obtained by Fourier integration from the total pair correlation functions, and the solid red line correspond to the total structure factor as obtained by direct calculation in the reciprocal space. The comparison with experiments is based on the results of Ref. [54].

yielding the best peak positions and intensities, in particular for the first minimum, greatly improved when the vdW corrections are included. This is contrasted by the PBE case for which the first minimum is much less pronounced and only partially corrected by the vdW inclusion. The corresponding R_χ values are 17.4% (BLYP), 16.1% (BLYP-vdW), 24.5% (PBE), and 21.6% (PBE-vdW).

A word of caution is needed when analyzing the behavior of model 3 in reciprocal space. While it remains true that BLYP performs better than PBE in reproducing the profile of the structure factor over the entire range of high k values, an increase of the main peak intensity is observed in the BLYP case after inclusion of the vdW contributions, thereby worsening the agreement with experiments. Indeed, we obtain R_χ values larger for BLYP-vdW, i.e., 7.3% (BLYP) and 7.9% (BLYP-vdW). To elucidate this issue, we recall that the total structure factors shown in Fig. 1 and Fig. 2 have been obtained via Fourier integration from the total pair correlation functions. Alternatively, one can resort to the direct calculation of the structure factors, in spite of the noisy profile often exhibited for disordered systems when the statistics is limited to a single trajectory. By applying this methodology one obtains the results shown in Fig. 3, featuring R_χ values equal to 10.3% (BLYP) and 9.8% (BLYP-vdW). Therefore, the inclusion of vdW effect can also improve (albeit to a limited extent) the BLYP description of a-$GeTe_4$ in reciprocal space.

B. Partial pair correlation functions

Having established the performances of the different schemes in reproducing measurable quantities in reciprocal and direct space, one can focus on the atomic structure and the related coordination environment of the a-$GeTe_4$ models. Hereafter we shall refer to model 1 (PBE, PBE-vdW) and model 3 (BLYP, BLYP-vdW). In Fig. 4 the partial pair correlations function $g_{\rm GeTe}(r)$ appears barely sensitive to the

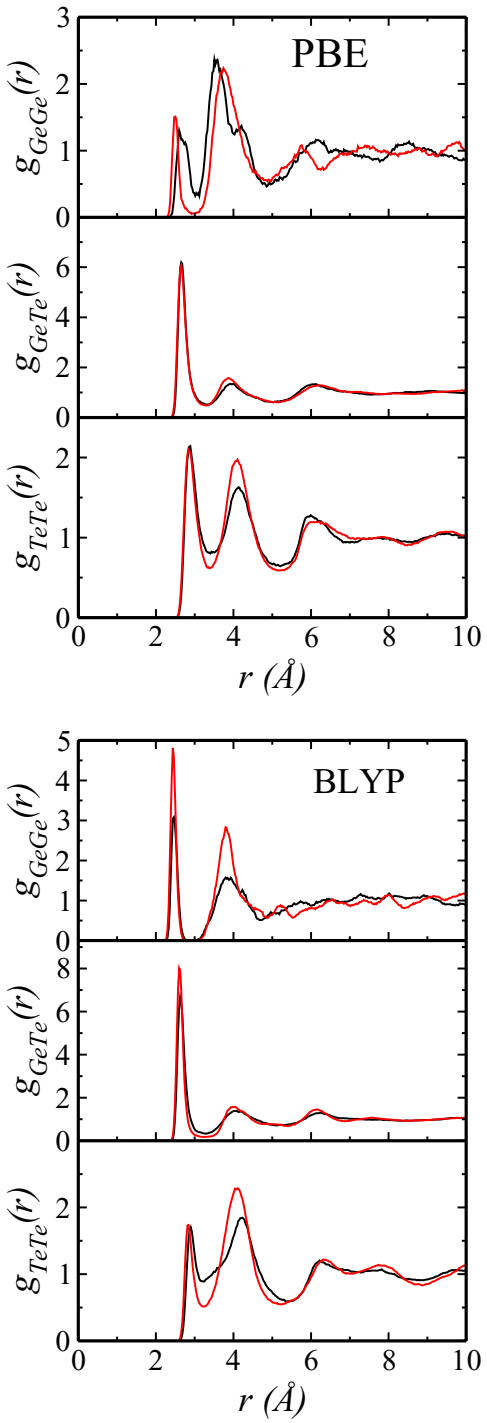

FIG. 4. (Color online) Partial pair distribution functions of $GeTe_4$ glass for the $g_{GeGe}(r)$, $g_{GeTe}(r)$, and $g_{TeTe}(r)$ from the top to the bottom panel, respectively. PBE and BLYP results. Results without VdW are the black lines and with vdW the red lines.

specific details of the electronic structure description (XC functional and inclusion of vdW contribution). The only noticeable feature is the increase of the intensity of the first main peak when comparing BLYP and BLYP-vdW.

The situation changes drastically for Ge-Ge correlations. In this case, the vdW contributions have a profound effect on the Ge environment. In the PBE case, the second peak (at 3.5 Å) and the third peak (at about 4 Å) merge due to the decrease in the relative number of Ge involved in edge-sharing connections and the marked increase of the corner-sharing counterpart (Table I).

TABLE I. Percentages of Ge and Te atoms involved in homopolar bonds (N_{GeGe} and N_{TeTe}), together with the percentages of Ge atoms involved in corner-sharing (CS) and edge-sharing (ES) connections. We also provide the percentages of Ge and Te atoms involved in fourfold and twofold coordinations, respectively. A cutoff of 3 Å is adopted throughout.

	N_{GeGe}	N_{TeTe}	N_{Ge}^{CS}	N_{Ge}^{ES}	4-fold Ge	2-fold Te
PBE	26.3	85.6	34.7	39.0	68.6	57.5
PBE+VdW	16.0	87.9	65.6	18.4	67.3	55.8
BLYP	25.9	73.6	62.8	11.3	76.8	64.8
BLYP+VdW	30.3	72.5	53.0	16.6	85.9	73.9

The number of Ge-Ge homopolar bonds also decreases, resulting from a narrow profile of the peak at 2.5 Å. We recall that our counting rule for the edge and corner connections is based on three kinds of Ge atoms, those involved in fourfold rings, indicative of edge-sharing motifs, those involved in homopolar bonds, the remaining being associated with corner-sharing links. Focusing on the BLYP and BLYP-vdW results on $g_{GeGe}(r)$, there is an increase in the peak intensities and the absence of any shoulder in between 3.5 Å and 4 Å, while the vdW part provides a more structured organization in shells of Ge neighbors. The number of homopolar bonds increases after inclusion of the vdW contribution, partially at the expenses of the number of Ge atoms involved in corner-sharing connections. This has an effect on the overall network topology, as will be detailed further in the section (Sec. III D) devoted to the bond angle distributions.

The pair correlation function $g_{TeTe}(r)$ is the most sensitive to both the XC functional and the vdW inclusion. Profound changes are encountered when using the XC BLYP instead of PBE (relative intensities of the two main peaks and sharpness of the first minimum, especially in the absence of vdW contributions). There is higher number of Te-Te linkages in the PBE case, while the shapes of the pair correlations functions become similar for intermediate range distances ($r > 6$ Å). Mostly affected by the vdW contributions is the BLYP case, for which a deep first minimum shows up between two peaks of enhanced intensities. Based on the above, one expects that the PBE and BLYP subnetwork topologies of Te are more dissimilar than the Ge ones.

To conclude this section, we underline that the availability of the partial pair correlation functions allows us to capture the origins of the shape exhibited by the total pair correlation function as obtained within BLYP (Fig. 2). A small shoulder is indeed visible when following the profile of the first peak. In Fig. 5 this feature is rationalized in terms of the decomposition in the two main contributions to the total pair correlation function, namely $g_{TeTe}(r)$ and $g_{GeTe}(r)$ [this shoulder occurs around the first minimum position of the $g_{GeGe}(r)$ which makes the contribution of this latter immaterial]. In the BLYP case, the shoulder manifests itself due to the combined effects of the main peak profiles in $g_{GeTe}(r)$ and $g_{TeTe}(r)$.

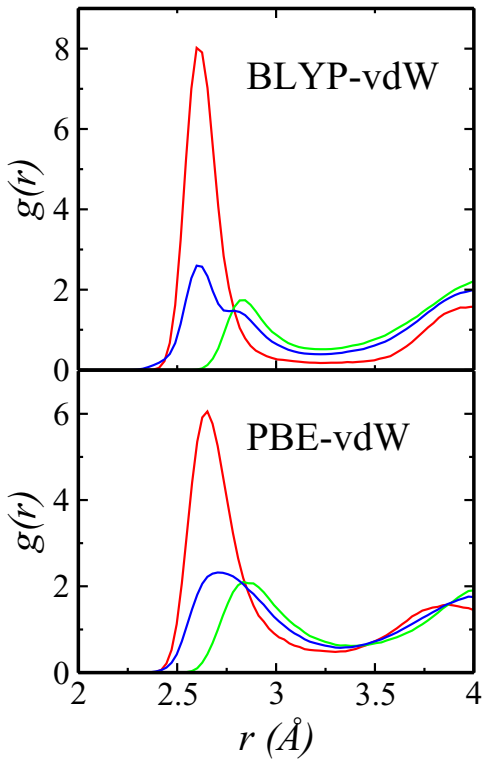

FIG. 5. (Color online) Partial pair distribution functions of $GeTe_4$ glass for the $g_{GeTe}(r)$ (red lines), $g_{TeTe}(r)$ (green lines), and $g_{tot}(r)$ (blue lines). Results are shown for BLYP-vdW (top panel) and PBE-vdW (bottom panel).

C. Coordination number and analysis of local environment

We enrich the findings provided by the pair correlation functions by collecting information on the nearest-neighbor bond distances for the four models. We give also the value of the partial coordination numbers obtained by integration of the pair correlation function up to the first minimum (Table II). First, we define c_{Ge} and c_{Te} as the concentration of each species. The average coordination number $\bar{n}$ is defined as $\bar{n} = c_{Ge}n_{Ge} + c_{Te}n_{Te}$, where n_{Ge} and n_{Te} are the coordination numbers of Ge and Te. These, in turn, are given by $n_{GeGe} + n_{GeTe}$ and $n_{TeTe} + n_{TeGe}$, respectively, with $n_{GeTe} = 4n_{TeGe}$. For each one of the bond distances, values are within 2% for the four models, with the notable exception of r_{GeGe}, higher by as much as 7% in the PBE case. Looking at the coordination number n_{GeGe}, the different PBE, PBE-vdW, BLYP, and BLYP-vdW values (all found to lie within 0.21) are the mere consequence of the different shapes and intensities of the peaks associated with homopolar bonds.

TABLE II. Bond distances r_{ij} (in Å) in terms of position of the first maximum of the pair correlation functions g_{ij}, partial coordination numbers n_{ij} obtained by integration of g_{ij} up to the first minimum, coordination numbers n_i, and average coordination number $\bar{n}$. Note that for a tetrahedral chemical ordered network $\bar{n}$ is equal to 2.4. The results of PBEsol+vdW are from Ref. [12].

	PBE	PBE+vdW	BLYP	BLYP+vdW	PBEsol+vdW
r_{GeGe}	2.67	2.49	2.46	2.43	2.48
r_{GeTe}	2.65	2.65	2.62	2.59	2.64
r_{TeTe}	2.88	2.83	2.89	2.84	2.90
n_{GeGe}	0.27	0.16	0.28	0.37	0.33
n_{TeGe}	1.07	1.05	0.96	0.91	0.96
n_{TeTe}	2.71	2.47	1.60	1.40	1.94
n_{Ge}	4.54	4.35	4.14	3.97	4.17
n_{Te}	3.78	3.51	2.57	2.31	2.90
$\bar{n}$	3.93	3.68	2.87	2.65	3.15

The values of n_{TeTe} are indicative of quite different coordination neighborhoods when comparing BLYP and PBE (2.71, 2.47 PBE vs 1.60, 1.40 BLYP). In both the PBE and BLYP cases, consideration of the vdW parts reduces n_{TeTe}, as a result of the sharper profiles for the first minimum of the related pair correlation functions. By and large, it appears that BLYP coordination numbers are closer to those typical of a chemically ordered tetrahedral arrangement for this composition ($n_{GeGe} = 0, n_{GeTe} = 4, n_{TeTe} = 1, n_{TeGe} = 1$), this trend being enhanced by the vdW contribution. The large values of n_{TeTe} in the PBE case (2.71, 2.41) are a sign of strong departures from a tetrahedral network. Indeed, in a chemically ordered tetrahedral network, the Te atoms could either be part of $GeTe_4$ tetrahedra, form Te_n chains, or cross-link tetrahedra and chains. In Refs. [26,56], the labels AA, BB, and AB were introduced to describe these three environments. Such topologies are all compatible with an average $n_{TeTe} = 1$, definitely much smaller than what is found in the PBE case. On the other hand, the BLYP values for n_{TeTe} (1.60, 1.40) are somewhat closer to 1, showing the trend toward a tetrahedral arrangement when moving from PBE to BLYP. This specific effect of the BLYP recipe is in line with previous findings on GeSe systems. It was shown that BLYP reinforces the tetrahedral arrangement when compared to other exchange-correlation functionals (such as the Perdew-Wang one) based on the local density approximation as a reference starting point [29].

Table I collects further information on the network topologies. The percentage of Te atoms involved in homopolar bonds features higher values in the PBE case, in a way consistent with n_{TeTe} coordination numbers in between 2 and 3. Since using BLYP allows us to approach the tetrahedral order, the number of homopolarly bonded Te atoms decreases from ∼85% to about 70%. This is exactly what happens in the case of the (essentially) tetrahedral chemically ordered glassy $GeSe_4$ with a fraction of homopolarly bonded Se-Se atoms close to 70% [25,26].

D. Bond angle distributions

The bond angle distribution of Ge-Te-Ge angles, shown in Fig. 6, reflects the relative amount of corner- and edge-sharing connections. The predominance of corner-sharing connections, inherent in the BLYP approach (see Table I), is restored within PBE by inclusion of vdW forces. Accordingly, the bond angle distribution Ge-Te-Ge exhibits clear changes when going from PBE to PBE-vdW. In the absence of vdW contributions, there is one peak at about 80° followed by a less intense shoulder. In the PBE-vdW case, one observes a shift of the peak position to ∼90°, indicative of increased corner-sharing connections. There are also changes occurring

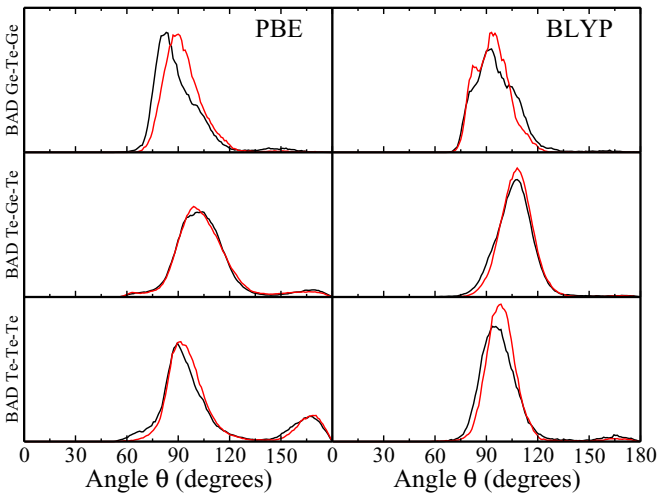

FIG. 6. (Color online) Bond angle distribution (BAD) Ge-Te-Ge, Te-Ge-Te, and Te-Te-Te. Left panels refer to PBE calculations (model 1) and right panels to BLYP calculations (model 3). Black lines correspond to the neglect of vdW corrections and red lines to the inclusion of vdW corrections.

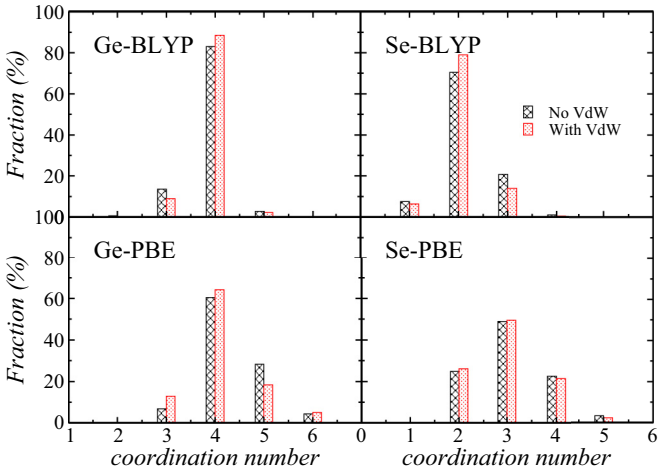

FIG. 7. (Color online) Fraction of n-fold Ge and n-fold Te atoms ($n = 1, 2, 3, 4, 5$, or 6) as calculated within BLYP model 3 and PBE model 1.

in the shape of Ge-Te-Ge bond angle distribution when comparing the BLYP and the BLYP-vdW results. The higher ratio between edge-sharing and corner-sharing connections (BLYP-vdW) favors the appearance of a distinct, edge-sharing related first peak. Also, the distribution vanishes more rapidly after the second, higher peak, to indicate that nontetrahedral connections are less important for the BLYP-vdW case.

The comparison of models obtained within different XC functionals shows that the bond angle distribution Te-Ge-Te changes drastically from PBE to BLYP, with the main peak shifting to higher value (108°) in the BLYP case. This has to be correlated with the onset of tetrahedral configurations. The small peak near 180° appearing in the PBE-vdW case is consistent with the existence of a small fraction of fivefold Ge sites. Indeed, peaks around 180° are a sign of octahedral-like structures. The inclusion of vdW dispersion forces has nearly negligible effects on the intrapolyhedra bond angle (Te-Ge-Te), due to the radial correction character of vdW interactions.

The bond angle distribution for PBE (Te-Te-Te) exhibits two mains peaks centered around 90° and 180°, respectively, while in the BLYP-vdW case only one single peak appears. These peaks can be ascribed to the presence of Te chains composed of at least three Te atoms, one of them having clearly two Te atoms as nearest neighbors. Also, the 180° angle can be regarded as a sign of a more important octahedral contribution.

E. Analysis of network topologies: Octahedral vs tetrahedral

The concepts expressed above on the topologies of the four models are exemplified by the local environment analysis of the n-fold Ge and n-fold Te atoms displayed in Fig. 7. The account of vdW forces leads to an enhanced structural organization for both the XC functionals, through an increase of the fractions of fourfold Ge and twofold Te. However, the network topologies are substantially different when comparing PBE and BLYP. In the PBE case, a sizable fraction of miscoordinated Ge atoms do exist at variance with the BLYP case. A closer analysis reveals that both BLYP-vdW and PBE-vdW do favor mainly fourfold-coordinated Ge sites and have close percentages of threefold contributions. However, PBE-vdW (as PBE) is characterized by fivefold Ge atoms in nonnegligible amounts. For Te, the twofold coordination is by far not the most important both for PBE and PBE-vdW. Threefold, fourfold, and even fivefold atoms are present together with twofold ones.

To better quantify the specific atomic coordinations, we used the local order parameter defined as

$$q = 1 - \frac{3}{8}\sum_{k>i}\left[\frac{1}{3} + \cos\theta_{ijk}\right]^2, \tag{5}$$

where θ_{ijk} is the angle formed between a central atom j and its neighboring atoms i and k. This order parameter [57,58] was averaged over the whole trajectory at 300 K and can vary between 0 and 1. Specifically, a value of $q = 1$ refers to the ideal tetrahedral network, while $q = 0$ indicates sixfold-coordinated octahedral sites. Values in between 0 and 1 are typical of a given defective octahedral configuration. This allows us to discriminate between different geometrical arrangements of atoms surrounding a given site. The results are displayed in Fig. 8 for the PBE-vdW and BLYP-vdW models. In our calculations, the maximum cutoff distance between two given atoms corresponds to the first minimum position in the corresponding partial pair correlation function.

The PBE results are compatible with a wide range of possible coordination environments. More precisely, in addition to perfectly sixfold octahedral sites ($q \sim 0$), defective octahedra lacking either one or two sites appear as overlapping broad peaks at $q = 0.30$ and 0.45. Distorted octahedral-like configurations featuring three nearest neighbors are also visible as a shoulder at $q = 0.75$, while a main peak, centered at $q = 0.95$, corresponds to the ordinary tetrahedral configuration. At variance with PBE, BLYP calculations do not feature any octahedral sites and the distribution takes zero values for $q < 0.18$. Then, for larger q, a broad peak centered around $q = 0.38$ appears, to be ascribed to defective

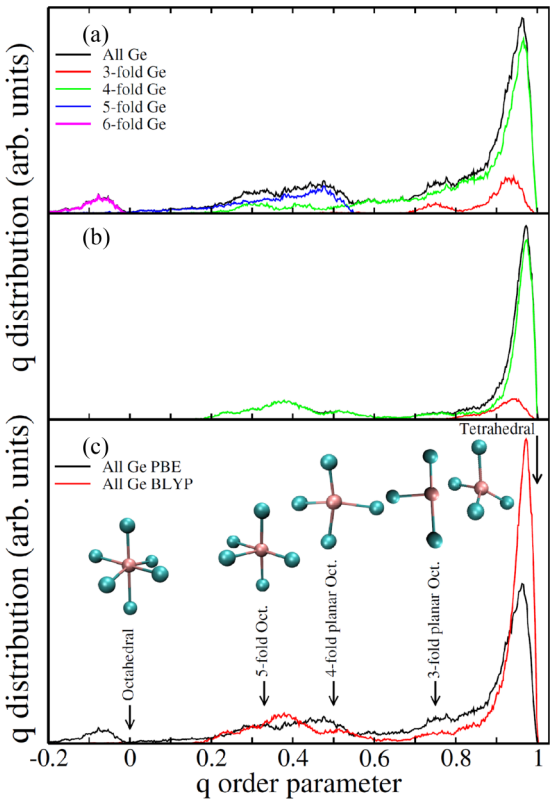

FIG. 8. (Color online) Distribution of the local atomic coordination motifs as a function of the order parameter q defined in the text. The total local order parameter distribution is obtained for (a) model 1 (PBE-vdW) and (b) model 3 (BLYP-vdW). The colored lines show the breakdown of the total distribution into the contributions of n-fold Ge atoms ($n = 3$, 4, 5, and 6). In panel (c) we provide the comparison between the total local order parameter distribution for model 1 (PBE-vdW) and model 3 (BLYP-vdW). The arrows are indicative of the exact q value of tetrahedral, octahedral, and some defective octahedral geometries. The distribution is normalized with respect to the number of Ge atoms.

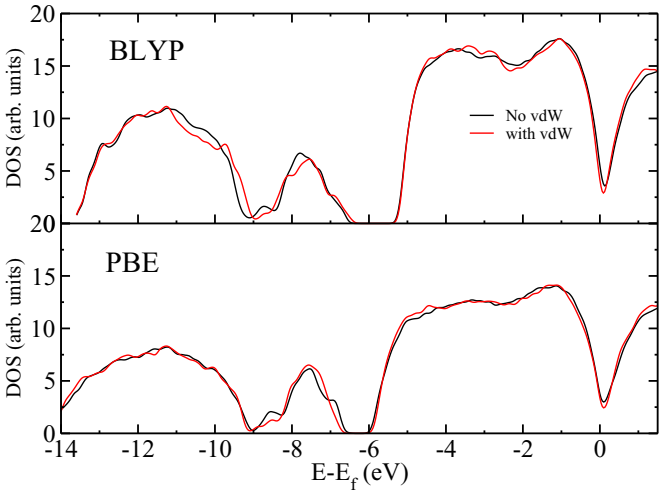

FIG. 9. (Color online) The electronic density of states extracted from the Kohn-Sham eigenvalues. Result for amorphous $GeTe_4$. A Gaussian broadening of 0.08 eV has been employed.

octahedra. This feature is less structured and pronounced than in the PBE case, and yet it demonstrates the presence of few incomplete fourfold octahedra also within the BLYP approach. The principal peak at $q = 0.95$ is sharper and features a higher intensity, indicating a high degree of stability of the tetrahedra underlying the short-range geometrical environment of the amorphous phase of $GeTe_4$.

It has been shown that integrating the peak of the fourfold Ge local order distribution in the range between 0.8 and 1.0, one can obtain a good estimate of the Ge atoms involved in a tetrahedral configuration [59]. By following the same procedure we found values equal to 41.07% (PBE), 44.13% (PBE-vdW), 48.13% (BLYP), and 58.13% (BLYP-vdW).

F. Electronic properties

The shapes of the electronic densities of states (Fig. 9) do not allow us to highlight a clear-cut correlation between the structure resulting from a given theoretical scheme and the bonding properties. In particular, the pseudogaps visible in both BLYP and PBE cases (with or without vdW corrections) turns out to be very similar. The underestimate of the band gap (experimental value $E = 0.86$–0.93 eV [60]) is not unexpected within a DFT-GGA framework [61,62] and it is seen to occur in ionocovalent systems such as glassy chalcogenides [63].

It is worthwhile to seek further insight into the interplay between atomic structure and electronic properties by resorting to the Wannier formalism, based on the notion of Wannier function and centers WFC (the W label referring to these degrees of freedom). Recently, we have employed these quantities to infer the extent of covalent vs ionic nature of bonding in the context of a study focused on a-$GeSe_4$ and a-GeS_4 [52]. This has been achieved by relying on the correspondence between the distances identified in the atom-Wannier centers pair correlation functions $g_{GeW}(r)$ (for a-GeS_4 or a-$GeSe_4$), $g_{SeW}(r)$ (for a-$GeSe_4$), $g_{SW}(r)$ (for a-GeS_4), and specific WFCs.

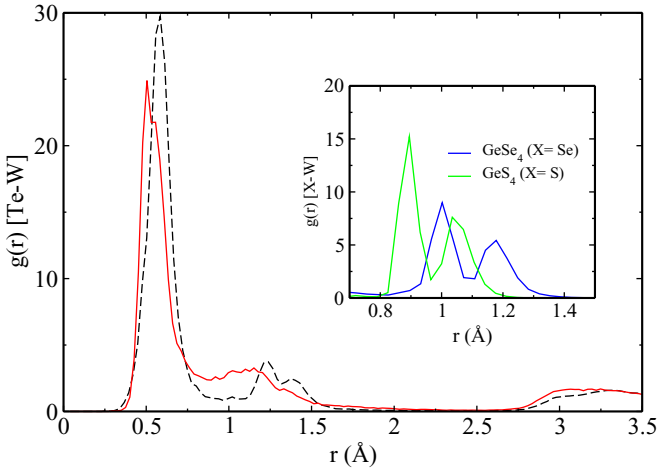

FIG. 10. (Color online) Partial pair correlation functions $g_{TeW}(r)$, where W stands for the coordinates of the Wannier centers. Black dashed lines refer to BLYP+vdW and red solid lines to PBE+vdW calculations. The inset highlights the double-peak feature in $g_{SeW}(r)$ and $g_{SW}(r)$ obtained in Ref. [52].

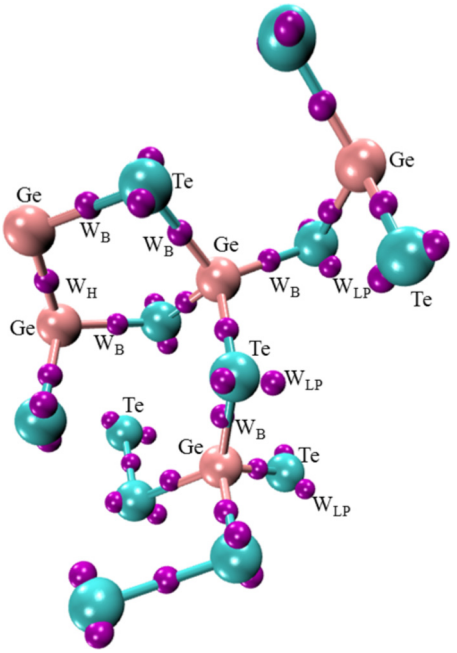

FIG. 11. (Color online) Details of the bonding environment for a-$GeTe_4$. For the color code, pink: Ge atoms, cyan: Te atoms, purple: Wannier centers (labeled as W). Only a few atoms are labeled along with representative Wannier centers. Three different Wannier centers can be distinguished. The first type, labeled as W_B, refers to the Ge-Te bonds. The second type, labeled as W_H, refers to homopolar Ge-Ge or Te-Te bonds. The third type, labeled as W_{LP}, indicates the lone pair (LP) valence electrons not participating in chemical bonds but remaining localized in the vicinity of the Te atoms.

Interestingly, a specific three-peak shape for $g_{Se(S)W}(r)$ was found to characterize the tetrahedrally bonded systems a-$GeSe_4$ and a-GeS_4, the peaks being due to Ge-Se(S) bonds, homopolar Se-Se (S-S) connections, and lone pair valence electrons (see the inset of Fig. 10). Figure 11 exemplifies the different location of the Wannier centers associated with these specific bonding and nonbonding situations for a given atomic configuration of a-$GeTe_4$ in the BLYP-vdW case.

In Fig. 10 we compare the $g_{TeW}(r)$ pair correlation function obtained within the BLYP-vdW and PBE-vdW frameworks. There is a striking analogy between the shape of $g_{TeW}(r)$(BLYP) and those of $g_{SeW}(r)$ and $g_{SW}(r)$ obtained in Ref. [52] by confirming the predominant tetrahedral network of the BLYP a-$GeSe_4$ model. On the contrary, in the PBE case, $g_{WTe}(r)$ takes a profile devoid of any double peak in between 1 Å and 1.5 Å, indicative of a large delocalization of the electron charge.

IV. CONCLUSIONS

Four models were considered to unravel the structure of glassy $GeTe_4$. The availability of results for two different exchange-correlation functionals, employed with or without van der Waals long-range corrections, is consistent with conclusive remarks developed along two different and yet complementary perspectives. These correspond to determining (a) the role of vdW dispersion forces for each one of the two XC functionals and (b) the role of the XC functional with or without the use of the vdW contribution. To achieve these goals, the basic criterion to reckon the validity of a given approach is the level of agreement between calculations and experiments for basic structural quantities, such as the total pair correlation function and the total structure factor.

Focusing on the (a) issue, it appears that the vdW contributions improve the total pair correlation function and the total structure factor in the PBE case and (less dramatically) also in the BLYP case. There is a systematic enhancement of the first minimum on $g(r)$, which corresponds to a lower total coordination number. Focusing on the partial pair correlation functions and the bond angle distributions, the effect is larger in the PBE case. For instance, within PBE, and after consideration of vdW forces, there is a striking increase in the number of corner-sharing connections at the expense of the edge-sharing ones. Compared to the case with no vdW, a moderate increase in the number of fourfold Ge atoms is also found.

Turning to the (b) issue, the best comparison with the available experimental probes is provided by the BLYP exchange-correlation functional, particularly when used in conjunction with the vdW forces. The resulting network is characterized by a dominant tetrahedral arrangement with minor contributions coming from the presence of coordination defects. Conversely, models obtained within PBE show a larger variety of local coordination environments with a coexistence of tetrahedral and octahedral motifs. The decreasing values taken by the total coordination number $\bar{n}$ when considering the four models, in the order PBE, PBE+vdW, BLYP, BLYP+vdW, are a revealing feature of such structural differences. Indeed, $\bar{n}$ moves down from 3.93, 3.68 (PBE) to 2.87, 2.65 (BLYP), approaching 2.4, i.e., the value for a chemically ordered network based on tetrahedra. In this context, our analysis of the local order parameter is instrumental in showing the substantial differences between the PBE and the BLYP networks.

Our results do confirm the importance of accounting for vdW dispersion forces when modeling Ge-Te chemical bonding in disordered binary chalcogenides. However, the mere account of vdW forces as an addition to a given exchange-correlation functional (such as PBE, taken to be the preferred choice of most practitioners so far) cannot by itself ensure the best performance of the selected DFT scheme. We demonstrate that the combination of BLYP and vdW forces leads to a better reproduction of available experimental properties, by promoting the establishment of a moderately defective tetrahedral network. This differs from early predictions based on the coexistence of two distinct arrangements (octahedral and tetrahedral) within the network structure of Ge-Te alloys at concentrations equal or close to $x = 0.2$.

ACKNOWLEDGMENTS

We acknowledge technical support from Romaric David and Michel Ringerbach (Pole HPC). We are grateful to the Direction Informatique (Pole HPC) of the University of Strasbourg for the access to computing resources. Some of the HPC resources were funded by the Equipex Equip@Meso project. We acknowledge partial support from GENCI under allocations DARI No. x2014095071, No. x2014096092, and No. 2014086045. We acknowledge financial support from the Agence National de la Recherche (ANR) within the framework of the project IRTeGlass No. ANR-14-CE07-0013-02.

[1] K. Makino, J. Tominaga, and M. Hase, Opt. Express **19**, 1260 (2011).
[2] A. Zaidan, V. Ivanova, and P. Petkov, Bulgarian Chem. Commun. **45**, 554 (2013).
[3] J. L. F. Da Silva, A. Walsh, and H. Lee, Phys. Rev. B **78**, 224111 (2008).
[4] S. Maurugeon, B. Bureau, C. Boussard-Plédel, A. Faber, P. Lucas, X. Zhang, and J. Lucas, Opt. Mater. **33**, 660 (2011).
[5] P. Lucas, C. Boussard-Pledel, A. Wilhelm, S. Danto, X.-H. Zhang, P. Houizot, S. Maurugeon, C. Conseil, and B. Bureau, Fibers **1**, 110 (2013).
[6] L. Run, T. Shi-Yu, B. Gang, Y. Qiao-Nan, L. Xue-Xin, X. Yi-Dong, Y. Jiang, and L. Zhi-Guo, Chin. Phys. Lett. **30**, 058101 (2013).
[7] H. Jiang, K. Guo, H. Xu, Y. Xia, K. Jiang, F. Tang, J. Yin, and Z. Liu, J. Appl. Phys. **109**, 066104 (2011).
[8] M. Chen, K. Rubin, and R. Barton, Appl. Phys. Lett. **49**, 502 (1986).
[9] M. Wuttig and N. Yamada, Nat. Mater. **6**, 824 (2007).
[10] M. Horie, N. Nobukuni, K. Kiyono, and T. Ohno, in *Optical Data Storage* (International Society for Optics and Photonics, 2000), pp. 135–143.
[11] J. Akola and R. O. Jones, Phys. Rev. Lett. **100**, 205502 (2008).
[12] K. Gunasekera, P. Boolchand, and M. Micoulaut, J. Appl. Phys. **115**, 164905 (2014).
[13] J. Kalikka, J. Akola, R. Jones, S. Kohara, and T. Usuki, J. Phys.: Condens. Matter **24**, 015802 (2012).
[14] M. Micoulaut, J. Chem. Phys. **138**, 061103 (2013).
[15] J. P. Perdew, A. Ruzsinszky, G. I. Csonka, O. A. Vydrov, G. E. Scuseria, L. A. Constantin, X. Zhou, and K. Burke, Phys. Rev. Lett. **100**, 136406 (2008).
[16] T. Björkman, Phys. Rev. B **86**, 165109 (2012).
[17] G.-X. Zhang, A. Tkatchenko, J. Paier, H. Appel, and M. Scheffler, Phys. Rev. Lett. **107**, 245501 (2011).
[18] R. Jonchiere, A. P. Seitsonen, G. Ferlat, A. M. Saitta, and R. Vuilleumier, J. Chem. Phys. **135**, 154503 (2011).
[19] J. Conesa, J. Phys. Chem. C **114**, 22718 (2010).
[20] F. L. Gervasio, M. Boero, and M. Parrinello, Angew. Chem., Int. Ed. Engl. **45**, 5606 (2006).
[21] S. Le Roux, A. Bouzid, M. Boero, and C. Massobrio, J. Chem. Phys. **138**, 174505 (2013).
[22] S. Le Roux, A. Bouzid, M. Boero, and C. Massobrio, Phys. Rev. B **86**, 224201 (2012).
[23] M. Micoulaut, S. Le Roux, and C. Massobrio, J. Chem. Phys. **136**, 224504 (2012).
[24] S. Le Roux, A. Zeidler, P. S. Salmon, M. Boero, M. Micoulaut, and C. Massobrio, Phys. Rev. B **84**, 134203 (2011).
[25] M. Micoulaut, A. Kachmar, M. Bauchy, S. Le Roux, C. Massobrio, and M. Boero, Phys. Rev. B **88**, 054203 (2013).
[26] K. Sykina, E. Furet, B. Bureau, S. Le Roux, and C. Massobrio, Chem. Phys. Lett. **547**, 30 (2012).
[27] K. Sykina, B. Bureau, L. Le Pollès, C. Roiland, M. Deschamps, C. J. Pickard, and E. Furet, Phys. Chem. Chem. Phys. **16**, 17975 (2014).
[28] C. Massobrio, M. Micoulaut, and P. S. Salmon, Solid State Sci. **12**, 199 (2010).
[29] M. Micoulaut, R. Vuilleumier, and C. Massobrio, Phys. Rev. B **79**, 214205 (2009).
[30] L. Giacomazzi, C. Masobrio, and A. Pasquarello, J. Phys.: Condens. Matter **23**, 295401 (2011).
[31] J. P. Perdew and Y. Wang, Phys. Rev. B **45**, 13244 (1992).
[32] R. Resta and S. Sorella, Phys. Rev. Lett. **82**, 370 (1999).
[33] N. Marzari and D. Vanderbilt, Phys. Rev. B **56**, 12847 (1997).
[34] R. Car and M. Parrinello, Phys. Rev. Lett. **55**, 2471 (1985).
[35] See http://www.cpmd.org/, copyright IBM Corp. 1990–2013, copyright MPI für Festkörperforschung Stuttgart 1997–2001.
[36] A. D. Becke, Phys. Rev. A **38**, 3098 (1988).
[37] C. Lee, W. Yang, and R. G. Parr, Phys. Rev. B **37**, 785 (1988).
[38] J. P. Perdew, K. Burke, and M. Ernzerhof, Phys. Rev. Lett. **77**, 3865 (1996); **78**, 1396 (1997).
[39] N. Troullier and J. L. Martins, Phys. Rev. B **43**, 1993 (1991).
[40] S. Grimme, J. Comput. Chem. **27**, 1787 (2006).
[41] F. Shimojo, Z. Wu, A. Nakano, R. K. Kalia, and P. Vashishta, J. Chem. Phys. **132**, 094106 (2010).
[42] K. Koizumi, M. Boero, Y. Shigeta, and A. Oshiyama, J. Phys. Chem. Lett. **4**, 1592 (2013).
[43] G. Ori, C. Massobrio, A. Bouzid, M. Boero, and B. Coasne, Phys. Rev. B **90**, 045423 (2014).
[44] P. Hohenberg and W. Kohn, Phys. Rev. **136**, B864 (1964).
[45] W. Kohn and L. J. Sham, Phys. Rev. **140**, A1133 (1965).
[46] J. Y. Raty, W. Zhang, J. Luckas, C. Chen, R. Mazzarello, C. Bichara, and M. Wuttig, Nat. Commun. **6**, 7467 (2015).
[47] S. Nosé, Mol. Phys. **52**, 255 (1984).
[48] S. Nosé, J. Chem. Phys. **81**, 511 (1984).
[49] W. G. Hoover, Phys. Rev. A. **31**, 1695 (1985).
[50] G. J. Martyna, M. L. Klein, and M. Tuckerman, J. Chem. Phys. **97**, 2635 (1992).
[51] P. E. Blöchl and M. Parrinello, Phys. Rev. B **45**, 9413 (1992).
[52] A. Bouzid, S. Le Roux, G. Ori, M. Boero, and C. Massobrio, J. Chem. Phys. **143**, 034504 (2015).
[53] M. Celino, S. Le Roux, G. Ori, B. Coasne, A. Bouzid, M. Boero, and C. Massobrio, Phys. Rev. B **88**, 174201 (2013).
[54] I. Kaban, T. Halm, W. Hoyer, P. Jovari, and J. Neuefeind, J. Non-Cryst. Solids. **326**, 120 (2003).
[55] A. C. Wright, J. Non-Cryst. Solids. **159**, 264 (1993).
[56] C. Massobrio, M. Celino, P. S. Salmon, R. A. Martin, M. Micoulaut, and A. Pasquarello, Phys. Rev. B **79**, 174201 (2009).
[57] J. R. Errington and P. G. Debenedetti, Nature (London) **409**, 318 (2001).
[58] P.-L. Chau and A. J. Hardwick, Mol. Phys. **93**, 511 (1998).
[59] S. Caravati, M. Bernasconi, T. D. Kühne, M. Krack, and M. Parrinello, Appl. Phys. Lett. **91**, 171906 (2007).
[60] P. Petkov, M. Wuttig, P. Ilchev, and T. Petkova, J. Optoelectron. Adv. Mater. **5**, 1101 (2003).
[61] H. Xiao, J. Tahir-Kheli, and W. A. Goddard, III, J. Chem. Phys. Lett. **2**, 212 (2011).
[62] B. G. Johnson, P. M. Gill, and J. A. Pople, J. Chem. Phys. **98**, 5612 (1993).
[63] L. Giacomazzi, C. Massobrio, and A. Pasquarello, Phys. Rev. B **75**, 174207 (2007).